



Weibull analysis of effect of T6 heat treatment on fracture strength of AM60B magnesium alloy

A. H. SHEVIDI, R. TAGHIABADI, A. RAZAGHIAN

Department of Materials Science and Ceramic Engineering, Imam Khomeini International University, Qazvin, Iran

Received 16 November 2016; accepted 4 April 2017

Abstract: The effect of T6 heat treatment on the fracture strength and reliability of AM60B alloy was studied. The tensile specimens were poured at three different temperatures of 670, 685 and 700 °C for different holding times of 5, 10 and 15 min. The fluidity test was also conducted to determine the fluidity length under different pouring temperatures and holding times. According to the results, the optimum pouring temperature and holding time were determined as 685 °C and 10 min, respectively. SEM fractography of the tensile specimens reveals that the entrained oxides and oxide-related porosities are the main factors responsible for the reduction of fracture strength under the non-optimal casting conditions. The Weibull statistical approach was used to quantify the scatter of fracture strength in as-cast and heat-treated conditions. For this purpose, T6 schedule was applied to the specimens prepared under the optimal casting condition. It is found that, despite minor effect on the average fracture strength, T6 heat treatment improves the reliability of castings, where the Weibull modulus is increased by 75%. According to the microstructural and fractography observations, this improvement is related to the evolution of more uniform microstructure and the elimination of coarse brittle β -particles in heat-treated samples.

Key words: Mg–Al alloy; AM60B alloy; die-cast; Weibull analysis; fracture strength; fluidity

1 Introduction

Due to their high specific strength, low density and good damping capacity, Mg high-pressure die-casting alloys have been widely studied and used for a wide range of applications, including aerospace and automotive industries [1–5]. Regarding to their fine-grain structure, strengthening effect exerted by second-phase particles, and supersaturation of the alloying elements, these alloys exhibit good mechanical properties and fracture toughness and, therefore, are not heat-treated conventionally [6,7]. Moreover, heat treatment may also affect the relative advantages of fine-grain structure and give rise to the surface blistering and formation of gas pore defects [6–8]. However, if done properly, it was shown that heat treatment is able to offer particular benefits for Mg–Al die-casting alloys including stress-relieving, dissolution of large and brittle particles like Mg–Mg₁₇Al₁₂ eutectic, and enhances their tensile properties and fracture toughness [8–10]. These alloys are conventionally subjected to T4 or T6 heat treatment process. A T4 temper involves a solution

treatment at 420 °C for 16–24 h followed by water quenching. A T6 temper, however, involves an identical thermal process with an additional aging treatment at 180 °C for 8 h [9,10].

One of the most challenging aspects of Mg casting alloys is their exceptional oxidation susceptibility in molten state, which together with non-protective vulnerable nature of their surface oxide, results in very high oxide inclusion contents of 10–20 times more as compared to the Al alloys [11–15]. The entrainment of magnesium surface oxides in the bulk of a molten alloy takes place as a result of a folding action in which two dry sides of the oxides are folded over each other. This process generates un-bonded oxide–oxide interfaces in solidified casting, which act as pre-existing cracks with some entrapped air in between [13,16–19].

Regarding to their industrial importance, extensive work has been done on the effect of entrained double oxides on the tensile properties and casting reliability of Al alloys [18–23]. However, so far, few studies have dealt with Mg alloys. MIRAK et al [13] studied the characteristic of Mg double-over oxides in AZ91 Mg alloy. They showed that the morphology of bifilms is

characterized by the amount of trapped air rather than their fold morphology. The effects of double-over oxides (bifilms) on the tensile properties and Weibull reliability of commercial purity Mg were also investigated by GRIFFITHS et al [16]. They indicated that the formation and entrainment of folded-over MgO films lead to the broader distribution of tensile properties.

Regarding to the exceptional oxidation susceptibility in a molten state, magnesium-based alloys are quite prone to the formation and entrainment of magnesium double oxides. It is believed that such oxide is one of the most important factors responsible for the scatter in fracture strength and reduction in castings reliability. Therefore, it is important to study the optimum casting parameters in order to obtain high quality castings with less entrained oxide inclusions. In this work, the effects of pouring temperature and holding time on the microstructure, distribution of casting defects and fracture strength of AM60B Mg–Al alloys were studied. Furthermore, in order to improve the reproducibility of the castings, the effects of T6 heat treatment on the fracture strength and Weibull reliability of the alloy were also studied.

2 Weibull analysis approach

The Weibull analysis approach is an effective tool for exploring the mechanical strength variability of the materials arising from their defects and structural flaws. In this approach, the weakest link theory is applied in such a way that the failure of one link, resulting from a flaw, may lead to a total failure. According to the three-parameter Weibull distribution, for an isotropic material (where the probability of the presence of a flaw in an arbitrary volume is similar throughout the material) containing N links, the probability of failure $F(x; \gamma, \alpha, \beta)$ at a loading stress of x for one link is [24–26]

$$F(x; \gamma, \alpha, \beta) = 1 - \exp\left[-\left(\frac{x-\gamma}{\alpha}\right)^\beta\right] \quad (\gamma \geq 0, \alpha \geq 0, \beta \geq 0) \quad (1)$$

where γ , α and β are location, scale and shape parameters, respectively. When $\gamma=0$, the two-parameter Weibull distribution is derived as follows:

$$F(x; \alpha, \beta) = 1 - \exp\left[-\left(\frac{x}{\alpha}\right)^\beta\right] \quad (\alpha \geq 0, \beta \geq 0) \quad (2)$$

In the context of this study, $F(x; \alpha, \beta)$ represents the probability that the fracture strength is equal to or less than x . Using the equality of $F(x; \alpha, \beta) + R(x; \alpha, \beta) = 1$, the probability of survival $R(x; \alpha, \beta)$, i.e., the probability that the fracture strength is at least equal to x , is defined as

$$R(x; \alpha, \beta) = \exp\left[-\left(\frac{x}{\alpha}\right)^\beta\right] \quad (\alpha \geq 0, \beta \geq 0) \quad (3)$$

Using linear regression method for estimating the scale and shape parameters, and taking logarithms twice, Eq. (2) is converted to a straight line form, Eq. (4), so the Weibull modulus (β) can be obtained from its slope:

$$\ln\{\ln[1/(1-F(x; \alpha, \beta))]\} = \beta \ln x - \beta \ln \alpha \quad (4)$$

It has been shown that the Weibull modulus is a better measure for material reliability than conventional statistics. Fracture strength values, which are determined from experimental work, are arranged in order as follows:

$$x_1 \leq x_2 \leq x_3 \leq x_i \leq x_n \quad (5)$$

There are several estimates for $F(x; \alpha, \beta)$. The one that is widely used for the j th fracture, from a total of N results, is

$$F(x; \alpha, \beta) = (j-0.5)/N \quad (6)$$

3 Experimental

The chemical composition of as-received AM60B ingots is presented in Table 1. The melting operation was done in a steel crucible using an electrical resistance furnace (3×400 V/50 Hz–60 kW). Protective atmosphere system was activated as soon as the charge temperature reached 400 °C and protected the liquid surface in an adiabatic environment by a gas mixture of 99.82% N₂ and 0.18% sulphur hexafluoride (SF₆). The melt was superheated up to the desired temperature of (670, 685, 700 °C), held for 5, 10 and 15 min and stirred gently before being poured. To have tensile samples (Fig. 1), the melt was poured into a preheated (250 °C) cast-iron tensile specimen mold (ASTM B 557M–02a). The average cooling rate of the mold was around 3 °C/s.

Table 1 Chemical composition of commercial AM60B alloy used in this work (mass fraction, %)

Be	Ni	Cu	Fe	Si	Mn	Zn	Al	Mg
0.0007	–	0.003	0.002	0.031	0.304	0.155	5.830	Bal.

The obtained samples were coded according to their preparation method as XXX/XX. The first part refers to the pouring temperature of the sample, and the second part (after the slash) refers to the holding time of the melt. To investigate the effect of T6 heat treatment on the fracture strength and the strength reliability, some of tensile specimens obtained under optimized casting condition were subjected to solution treatment at 420 °C for 24 h followed by water quenching at ambient temperature. The specimens then were artificially aged at 180 °C for 8 h. The tensile tests were conducted on a Zwick/Roell-Z100 universal testing machine at a crosshead speed of 0.5 mm/min. The average of four tests was reported as the final strength. Eighteen tension

tests were also carried out for statistical analysis of the fracture strength.

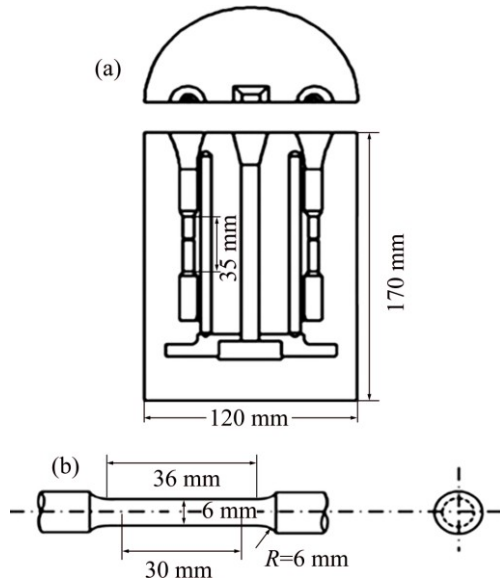


Fig. 1 Schematic diagram of cast-iron mold (a) and tensile test specimen (b)

The fluidity of the alloys was determined by a vacuum suction fluidity test apparatus (Fig. 2). The molten alloy with desired temperature, held isothermally for desired time after skimming and stirring, was sucked into the glass tube under the predetermined pressure of 27 kPa. After the solidification process was completed, the flow length of the alloy samples was measured as fluidity length. The average of four results was reported as the final fluidity length.

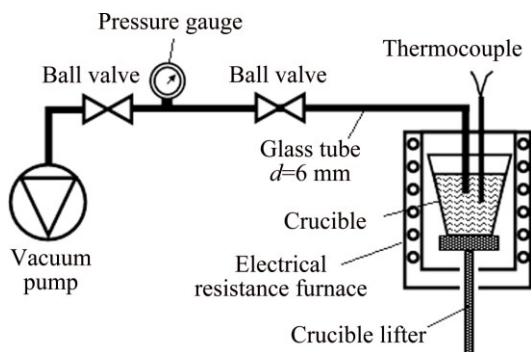


Fig. 2 Sketch of apparatus used for fluidity measurement

Samples for microstructural observations were prepared by standard metallographic procedures and each cross-section was etched using 20 mL acetic glycol + 1 mL acetic acid + 60 mL HNO₃ + 20 mL ethylene glycol + 19 mL distilled water reagent. 1% HF–distilled water reagent was also used to reveal the grain structure. The microstructure of the samples was studied by an Olympus optical microscope and a VEGA-TESCAN scanning electron microscope equipped with

the energy dispersive X-ray spectroscopy (EDS). The fracture surfaces of the tensile specimens were also studied by a scanning electron microscope.

4 Results and discussion

4.1 Effect of pouring temperature and holding time on microstructure and fracture strength of AM60B alloy

The variation of the fracture strength of AM60B alloy with the poring temperature for different holding times is shown in Fig. 3. It is seen that, regardless of the holding time, the fracture strength initially increases and reaches a maximum at the pouring temperature of 685 °C, and then decreases by further increase of temperature. It is also understood from the figure that the optimum condition is obtained at 685 °C after holding for 10 min.

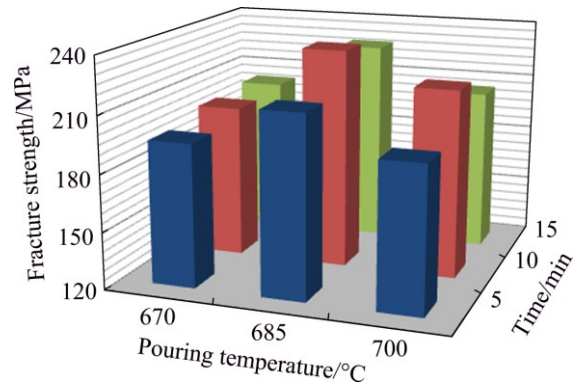


Fig. 3 Variation of fracture strength of AM60B alloy with pouring temperature for different holding times

Due to its low density ($\sim 1.8 \text{ g/cm}^3$) and specific heat capacity ($\sim 1 \text{ J/(g}\cdot\text{°C)}$) [27], AM60B alloy exhibits low metallostatic pressure and rapid solidification characteristics leading to its low mold-filling ability. Therefore, in the critical stage of alloy solidification, an appropriate balance between the pouring temperature and holding time is crucial to improve its fluidity and interdendritic feeding ability. Figure 4 illustrates the fluidity variation of AM60B alloy versus pouring temperature for different holding times. As expected, at a given holding time, the fluidity increased linearly with increasing pouring temperature because of the viscosity reduction. Increasing the holding time from 5 to 10 min also improved the fluidity, which can be attributed to the better temperature homogenization in the molten bath and probably settlement of the entrained magnesium oxides. Further increasing the holding time from 10 to 15 min, increased the fluidity at the lowest pouring temperature (i.e. 670 °C), but decreased it at the highest pouring temperature (i.e. 700 °C), which seemed to be due to the excessive formation and entrainment of magnesium oxide inclusions at higher temperatures.

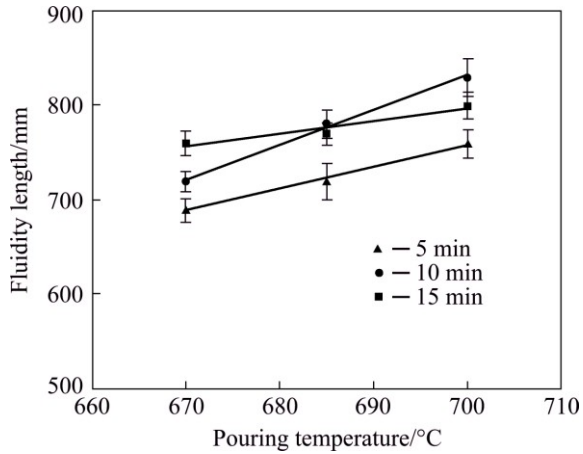


Fig. 4 Effect of pouring temperature and holding time on fluidity length of AM60B alloy

The as-cast microstructure of AM60B alloy is shown in Fig. 5(a). The presence of α -Mg dendrite cells and interdendritic/grain boundary β -Mg₁₇Al₁₂ with the EDS analysis shown in Fig. 5(b) is quite evident in the microstructure. The β -phase crystallization at

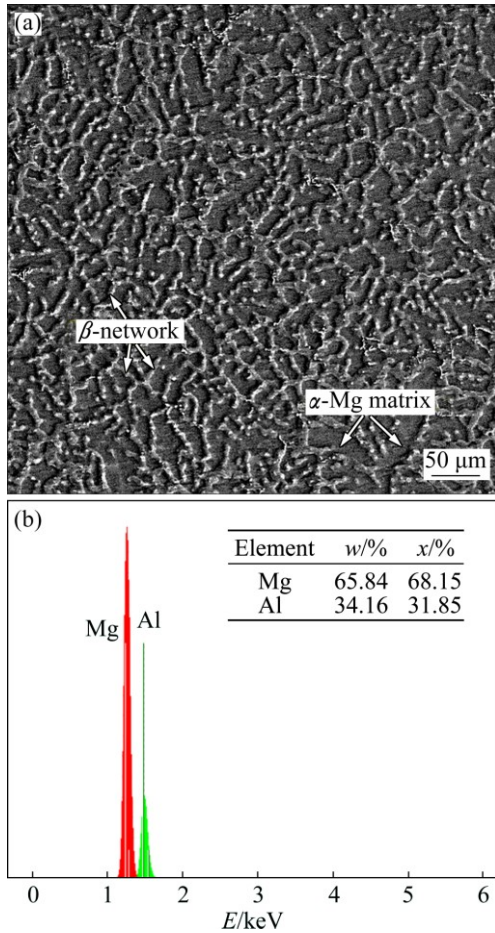


Fig. 5 SEM image of as-cast AM60B alloy showing interdendritic formation of β -Mg₁₇Al₁₂ network in α -Mg matrix (a) and EDS analysis of interdendritic β -Mg₁₇Al₁₂ compounds (b)

interdendritic regions is mainly due to the segregation of Al atoms in the liquid phase exiting in between the growing primary α -Mg dendrites and the subsequent eutectic reaction in the final stage of solidification, $L \rightarrow L + \alpha\text{-Mg} \rightarrow \alpha\text{-Mg} + \beta\text{-Mg}_{17}\text{Al}_{12}$ (Fig. 6) [28].

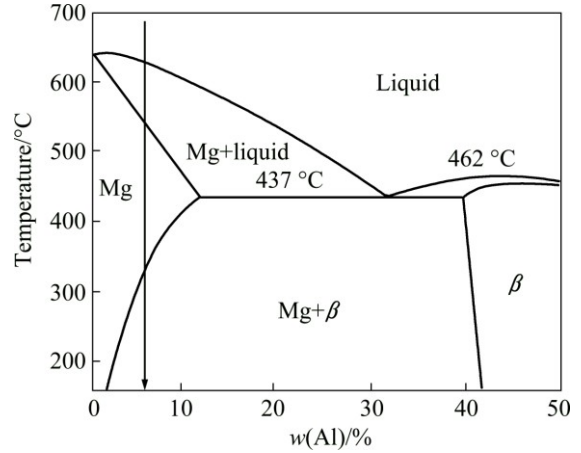


Fig. 6 Equilibrium Mg–Al phase diagram [28]

Figure 7 depicts the OM microstructure of the AM60B alloy at different pouring temperatures and holding time. The extensive formation of the large irregular-shaped porosities and the entrained bifilm oxides is quite evident in the microstructure of the specimens poured at 670 °C (Figs. 7(a–c)). Due to the protected melting and small difference (~28%) between the liquid and the solid state solubility of H₂ in Mg [29], hydrogen porosity is not a big issue in Mg alloys. Therefore, apart from the poor feeding ability of the molten alloy at lower temperatures (Fig. 4), the formation of these porosities, regarding to their specific morphologies, is thought to be associated with the existence of the entrapped magnesium oxides. Nonetheless, in agreement with the fracture strength results (Fig. 3), it seems that the higher the holding time is, the lower the fraction of entrained oxides (Figs. 7(a–c)). This is probably due to the higher fluidity of the molten alloy (Fig. 4) and the higher time available for oxides to exit the melt.

The bifilm oxide is normally trapped between the growing dendrite arms. As the alloy cools and contracts, the shrinkage stresses pull apart the dry un-bonded interface of the bifilm creating rather large interdendritic cavities through a mechanism known as ‘bifilm-assisted interdendritic porosity’ [17,29,30]. If, for example, due to the limited feeding ability and/or lack of residual melt, these cavities are not fed adequately, they convert to shrinkage porosities. Further diffusion of dissolved hydrogen atoms from the solidifying melt into the un-bonded interface of the bifilm may also overinflate the porosity (Figs. 7(a–c)) [17].

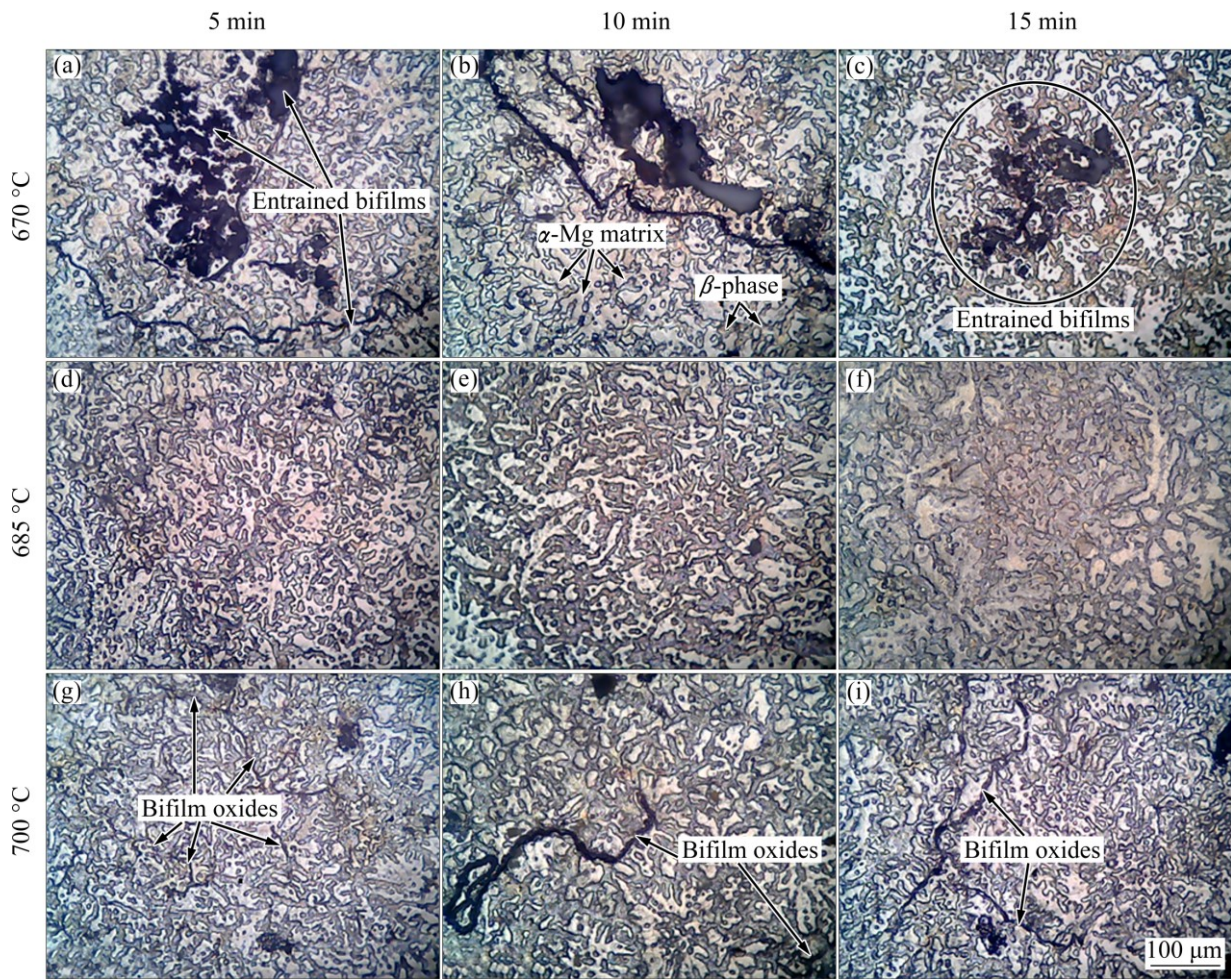


Fig. 7 OM microstructures of AM60B alloy poured at different pouring temperatures for different holding times

Figures 7(d–f) show the microstructures of the AM60B alloy poured at 685 °C. As can be seen, in agreement with its optimum feeding characteristic (Fig. 4) and high fracture strength (Fig. 3), the microstructure of the alloy at different holding times contains small amounts of dispersed micro-porosities. Figures 7(g–i) represent the microstructure of the AM60B alloy poured at 700 °C for different holding times. The formation of micro-pores and entrained double oxides in the microstructure is well evident. Increasing the holding time and pouring temperature over the optimum conditions of 10 min and 685 °C, results in the higher rates of magnesium oxidation which adversely affects the Be performance as a reactive element that is normally added to Mg alloys to increase their ignition temperature. Addition of Be also suppresses the oxidation progress of Mg alloys and improves the protection efficiency of the protective gas [11,12,31]. Therefore, again, it is reasonable to assume that the formation of micro-pores at 700 °C, at which the alloy naturally exhibits sufficient feeding ability (Fig. 4), is associated with the presence of the

entrained oxide inclusions.

The role of entrained oxides in the formation of micro-porosities and the premature fracture of the tensile specimens can also be assessed by the surface and subsurface study of the fractured samples, as shown in Figs. 8 and 9, respectively. Figure 8(a) shows the fracture surface of sample treated at 670 °C for 10 min. The presence of large porosities and entrained bifilm oxides is quite evident. In agreement with the optical microstructure (Fig. 7(a)), the presence of an entrained double-oxide film (Fig. 8(b)) just adjacent to the pore (as shown by the arrows) shows its impact on the formation of gas/shrinkage porosities. The OM micrograph taken from the subsurface regions of the fracture surface of this sample, shown in Fig. 9(a), also depicts the initiation of micro-cracks from a large tangled oxide as a crack initiator.

The fracture surface of sample treated at 685 °C for 10 min is shown in Fig. 8(c). As seen, in accordance to its good casting characteristics and high fracture strength, the fracture surface of this sample comprises localized ductile dimples and minor amounts of entrained

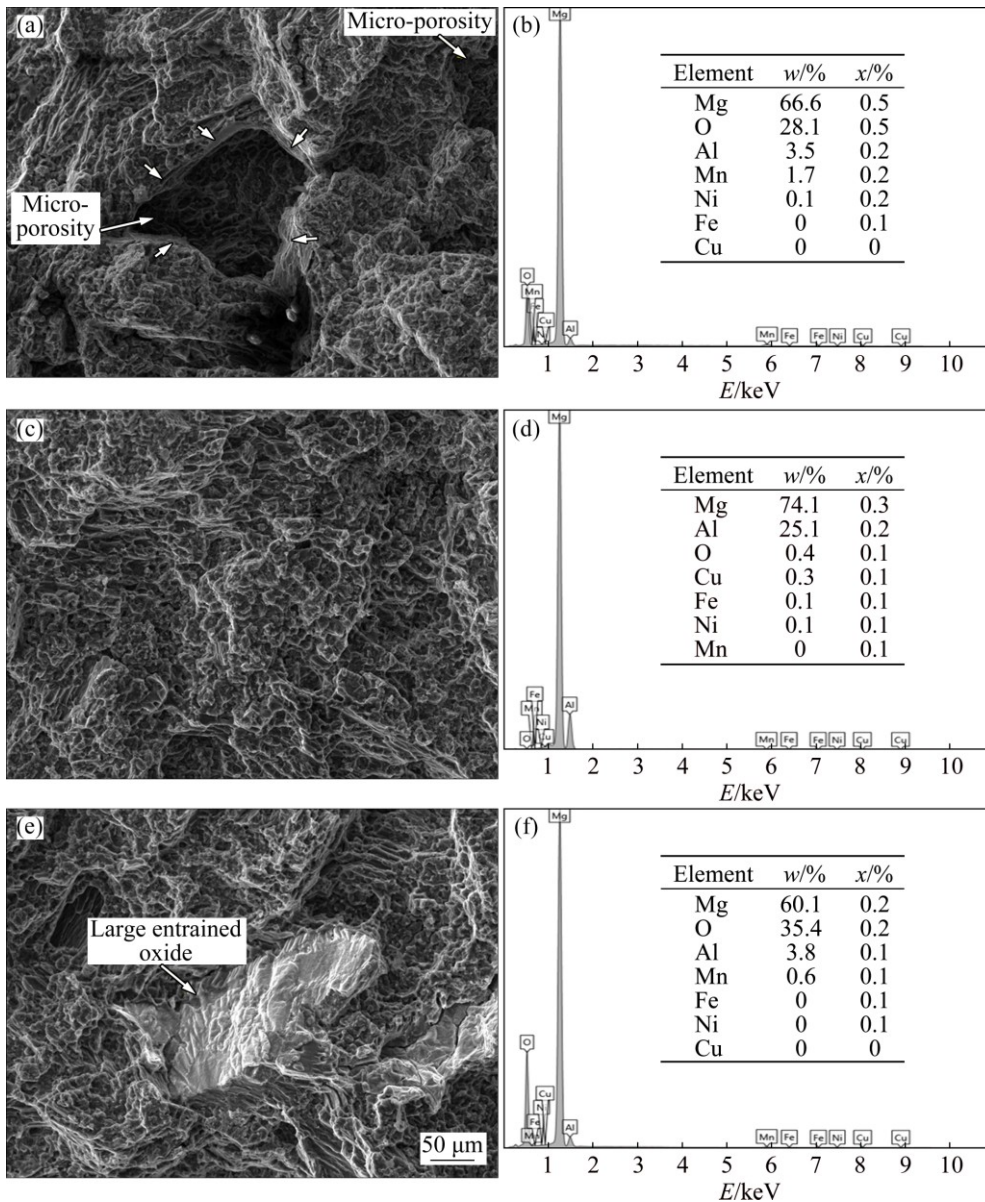


Fig. 8 SEM images of fracture surface (a, c, e) and corresponding EDS results (b, d, f) of samples treated at different conditions: (a, b) 670 °C, 10 min; (c, d) 685 °C, 10 min; (e, f) 700 °C, 10 min

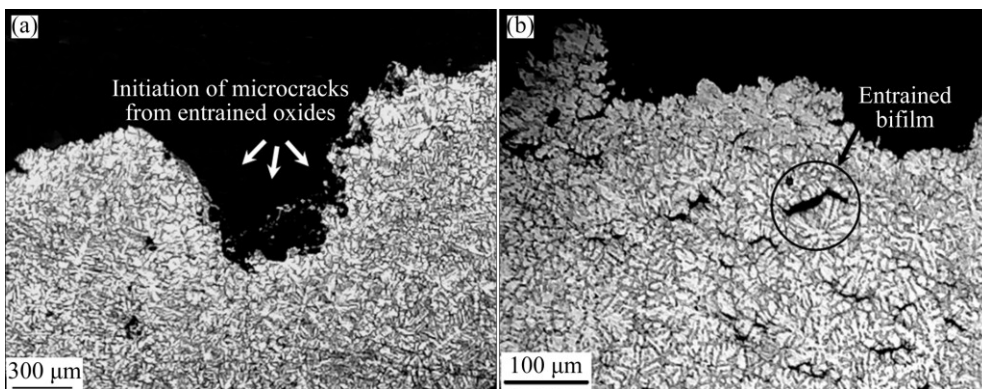


Fig. 9 OM micrographs taken from subsurface regions of fractured surfaces showing initiation of micro-cracks from large tangled oxide inclusion of sample treated at 670 °C for 10 min (a), and role of brittle β -compounds and entrained bifilm oxides in initiation of subsurface micro-cracks sample treated at 700 °C for 10 min (b)

oxides. The number and the average size of the pores also substantially decreased when compared to the sample treated at 670 °C for 10 min (Fig. 8(a)). The EDS microanalysis of the fracture surface (Fig. 8(d)) also demonstrates the lack of entrained oxides on the fracture surface of sample treated at 685 °C for 10 min. The fracture surface of sample treated at 700 °C for 10 min is shown in Fig. 8(e). The entrainment of a large bifilm oxide with the EDS analysis, shown in Fig. 8f, is quite evident on the surface which is thought to be the main factor leading to the premature fracture of this sample. Figure 9(b) also demonstrates how double oxides, as pre-existing micro-cracks, are opened out in the tensile direction leading to the formation of large subsurface microcracks in sample treated at 700 °C for 10 min.

4.2 Weibull statistical analysis of effect of heat treatment on fracture strength

As per tensile strength results (Fig. 3), the sample treated at 685 °C for 10 min was selected as the optimum choice to investigate the effect of T6 heat treatment on the reliability of fracture strength. The frequency histogram plots of the fracture strength for as-cast and heat-treated conditions are depicted in Fig. 10. The

corresponding plots of $\ln\{\ln[1/(1-F(x; \alpha, \beta))]\}$ versus \ln UTS (also referred to as Weibull distribution) are also shown in Fig. 11(a). The slope of the Weibull plots, known as Weibull modulus (β), actually shows the scale of the scatter/reliability in the data set. The higher the β value is, the less scattered the properties and the higher the reliability (or reproducibility).

It is also necessary to evaluate the applicability of the Weibull distribution for the obtained data. For this purpose, the critical value of R^2 ($\alpha=0.05$) should be calculated using the Eq. (7) proposed by TIRYAKIOGLU et al [32]:

$$R_{0.05}^2 = 1.0637 - \frac{0.4174}{n^{0.3}} \quad (7)$$

Equation (7) is valid for $5 < n < 100$. If R^2 of the linear regression from the Weibull probability plot is higher than $R_{0.05}^2$, then the Weibull distribution is applicable for the data. As in the present study, for $n=18$, the calculated $R_{0.05}^2$ is 0.888. Therefore, the R^2 values of the fitted lines for the as-cast and heat-treated samples (i.e. 0.974, and 0.961, respectively) are higher than $R_{0.05}^2$ which clearly means that the experimental data follow the Weibull analysis.

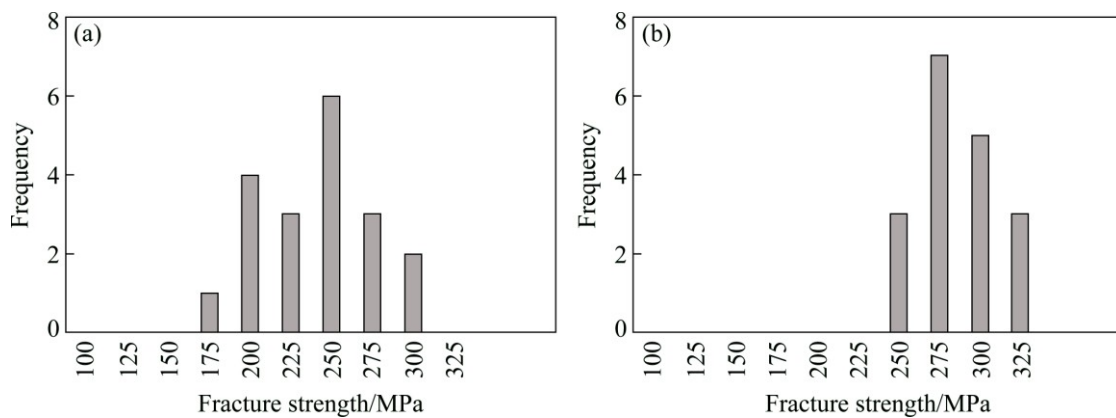


Fig. 10 Frequency histograms showing distribution of fracture strength for sample treated at 685 °C for 10 min under as-cast (a) and heat-treated (b) conditions

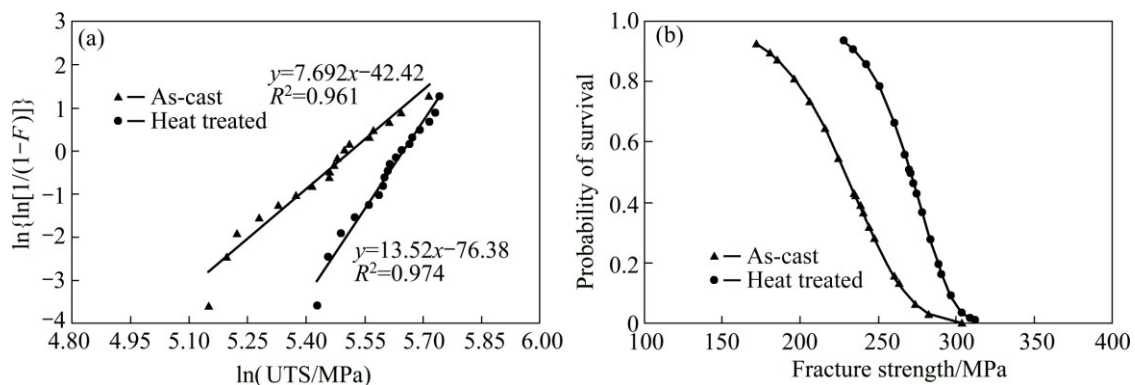


Fig. 11 Weibull plot of the fracture strength data (a), and probability of survival plot (b) of sample treated at 685 °C for 10 min in as-cast and heat-treated conditions

According to the statistical analysis results presented in Figs. 10 and 11(a) it is clear that T6 heat treatment does not have significant effects on the fracture strength of the AM60B alloy. In accordance to the previous findings [9], this behavior can be explained, to a certain extent, by the weak response of Mg–Al alloys to the age hardening process. It has been shown that the precipitation hardening process in Mg–Al based alloys exclusively comprises the formation of the equilibrium β -Mg₁₇Al₁₂ particles [9,33] that can act as potential barriers to dislocation motion, provided that they are finely distributed in the matrix [9,34]. Otherwise, the formation of coarse β -dispersoids increases the strength less than that which might be expected.

The effect of T6 heat treatment on the microstructure and grain structure of the AM60B alloy is shown in Figs. 12(a) and (b). As shown in Fig. 12(a), the continuous network of the β -Mg₁₇Al₁₂ phase (Fig. 5(a)) is mostly replaced by the relatively coarse discontinuous inter-grain and intra-grain β -dispersoids (see Fig. 12(a)) whose formation is explained by the high concentration of vacancies and relatively high diffusion rate of Al atoms in α -Mg matrix [9,33–35].

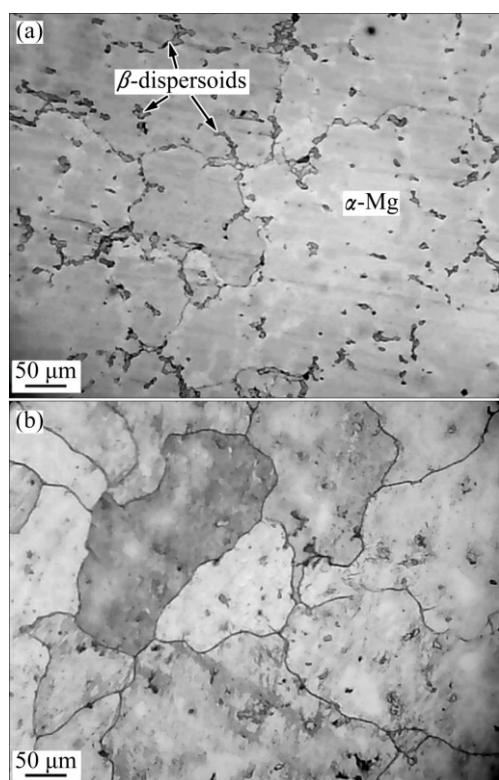


Fig. 12 OM microstructures of sample treated at 685 °C for 10 min under T6 condition: (a) Distribution of β -particles; (b) Grain structure

Dissolution of the β -network, on the other hand, is accompanied with the general coarsening of α -Mg grains as clearly seen in Fig. 12(b), where the average grain size

increases from (37.17 ± 11.10) μm in as-cast to (157.50 ± 38.13) μm in heat-treated condition. The grain boundaries themselves can act as potential barriers for dislocation movement [36,37] and according to the well-known Hall–Petch equation, the strength increases with reducing the grain size [38–40]. Therefore, the less improvement than that expected in the fracture strength of heat-treated samples can be explained by the weak age hardening response of the alloy and the softening effect caused by the grain coarsening phenomenon.

Despite its minor impact on the average fracture strength, dissolution of β -network in age-hardened samples gives rise to the higher Weibull modulus (β). According to Fig. 11(a), heat treatment has increased the β value by about 75% indicating that the heat-treated samples have less probability of fracture under the same level of applied load, as illustrated also in the ‘probability of survival’ plot (Fig. 11(b)). The probability of failure or reliability plot is a useful tool for determining the fracture probability of the castings under different levels of applied tensions. For instance, considering the reliability value of 0.95, it is possible to confirm from Fig. 11(b) that 160 and 220 MPa are reliable applied tensions for AM60B samples in as-cast and T6 heat-treated conditions, respectively.

The subsurface microstructure of fractured samples treated at 685 °C for 10 min under as-cast and heat-treated conditions, is shown in Fig. 13. It is clearly seen from Fig. 13(a) that, during tensile loading, the brittle β -Mg₁₇Al₁₂ particles are fractured, leading to the formation of subsurface micro-cracks that may become unstable and propagate through the material, which in turn, leads to the premature fracture of the sample. The propagation of micro-cracks in heat-treated samples preferentially occurs along the grain boundaries (Fig. 13(b)), but here, due to the isolated nature of discontinuous β -particles, micro-cracks growth may be effectively impeded by the ductile matrix giving rise to the enhanced tensile properties.

Based on the ‘weakest link theory’ of Weibull [24,25], the variation in fracture strength is generally linked to the structural defects present in the castings like gas or shrinkage porosities, brittle compounds and inclusions, and entrained oxides. As illustrated in Fig. 13(a), the micro-cracks almost always are originated from the β -compounds. Therefore, regarding to the similarity between the statistically investigated alloys in terms of their production route, it seems that the evolution of more uniform microstructure and the elimination of the coarse brittle β -particles, as potential crack initiator sites, can be emerged as the main factors associated with the higher reproducibility of heat-treated alloys.

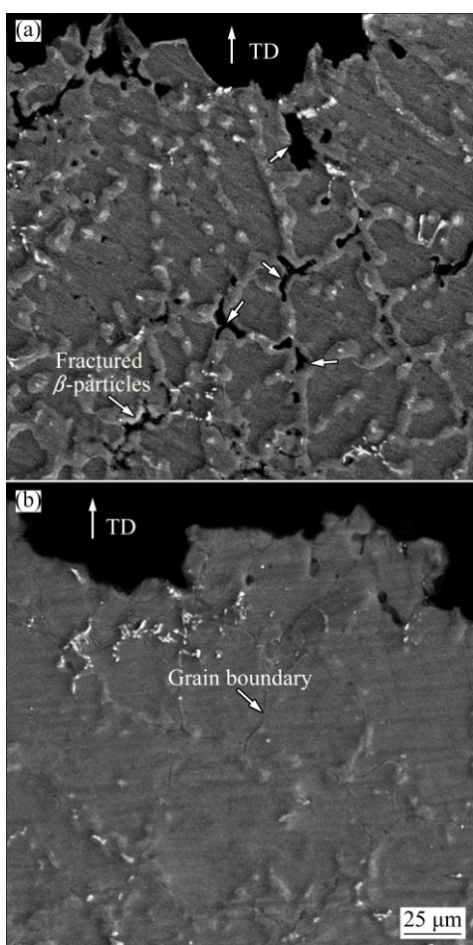


Fig. 13 Subsurface microstructures of fractured sample treated at 685 °C for 10 min under as-cast (a) and heat-treated (b) conditions (TD stands for tensile direction)

5 Conclusions

1) The proper selection of the casting parameters reduces the chance of entrained double oxides formation and oxide-related porosities, leading to enhanced fracture strength.

2) The formation of entrained double oxides and porosities adversely affects the fracture strength and increases its scatter or variability.

3) Despite minor effect on the fracture strength of AM60B alloys, T6 heat treatment has significant impacts on reliability of castings, where the Weibull modulus increased by 75%.

Acknowledgment

The authors would like to thank Magnesium-Gostar Arish Company, Qazvin, Iran, for providing the raw materials, melting equipments and technical support.

References

[1] LUO A. Magnesium casting technology for structural applications [J].

- Journal of Magnesium Alloys, 2013, 1: 2–22.
- [2] FISHER P A. Production, properties, and industrial uses of magnesium and its alloys [J]. *International Metals Review*, 23, 6: 269–285.
- [3] LIANG Song-mao, ZHANG Hua-wei, XIA Ming-xu, CHEN Rong-shi, HAN En-hou, FAN Zhong-yun. Microstructure and mechanical properties of die-cast Mg–Al–Ca alloy [J]. *Transactions of Nonferrous Metals Society of China*, 2010, 20: 1205–1211.
- [4] WANG L, CHEN T, JIANG W, FENG Y, ZHU Y. Microstructure and mechanical properties of AM60B magnesium alloy prepared by cyclic extrusion compression [J]. *Transactions of Nonferrous Metals Society of China*, 2013, 23: 3200–3205.
- [5] KINER K U. *Magnesium alloys and technologies* [M]. Weinheim, Germany: Wiley-VCH GmbH & KGaA, 2003.
- [6] SUMAN C. Heat treatment of magnesium die-casting alloys AZ91 and AM60B [C]//*Proc SAE Int Cong Expos*. Detroit, Michigan, 1989: 890207.
- [7] WANG X J, ZHU S M, EASTON M A, GIBSON M A, SAVAGE G. Heat treatment of vacuum high pressure die cast magnesium alloy AZ91 [J]. *International Journal of Cast Metals Research*, 2014, 27(3): 161–166.
- [8] CZERWINSKI F, KASPRZAK W. Heat treatment of magnesium alloys-current capabilities [J]. *Materials Science Forum*, 2013, 765: 466–470.
- [9] NIE J F. Precipitation and hardening in magnesium alloys [J]. *Metallurgical and Materials Transaction A*, 2012, 43: 3891–3939.
- [10] JIANGUO P, QUDONG W, MANPING L, YONGJUN C, WENJIANG D, SUÉRY M, BLANDIN J J. Effects of heat treatment on microstructure and mechanical properties of rolled AM50+xCa magnesium alloys [J]. *Materials Science Forum*, 2005, 488–489: 257–260.
- [11] SIN S L, ELSAYED A, RAVINDRAN C. Inclusions in magnesium and its alloys: A review [J]. *International Materials Review*, 2013, 58(7): 419–436.
- [12] BALART M J, PATEL J B, FAN Z. Melt protection of Mg–Al based alloys [J]. *Metals*, 2016, 131(6): 1–11.
- [13] MIRAK A R, DIVANDARI M, BOUTORABI S M A, CAMPBELL J. Oxide film characteristics of AZ91 magnesium alloy in casting conditions [J]. *International Journal of Cast Metals Research*, 2007, 20(4): 215–220.
- [14] CHEN Hu-kui, GONG Zan-fang. Oxidation behaviour of molten ZK60 and ME20 magnesium alloys with magnesium in 1,1,1,2-tetrafluoroethane/air atmospheres [J]. *Transactions of Nonferrous Metals Society of China*, 2012, 22: 2898–2905.
- [15] BALART M J, FAN Z. Surface oxidation of molten AZ31, AM60B and AJ62 magnesium alloys in air [J]. *International Journal of Cast Metals Research*, 2014, 27(5): 301–311.
- [16] GRIFFITHS W D, LAI N W. Double oxide film defects in cast magnesium alloy [J]. *Metallurgical and Materials Transaction A*, 2007, 38: 190–196.
- [17] CAMPBELL J. Entrainment defects [J]. *Materials Science and Technology*, 2006, 22(2): 127–145.
- [18] GOPALAN R, PRABHU N K. Oxide bifilms in aluminium alloy castings—A review [J]. *Materials Science and Technology*, 2011, 27, 12: 1757–1769.
- [19] CAMPBELL J. *Castings* [M]. 2nd ed. Oxford, UK: Butterworth-Heinemann, 2003.
- [20] LIU Shan-guang, CAO Fu-yang, YI Jun-ying, ZHAO Xin-yi, ZENG Jing, NING Zhi-liang, SUN Jian-fei. Effect of depressurizing speed on mold filling behavior and entrainment of oxide film in vacuum suction casting of A356 alloy [J]. *Transactions of Nonferrous Metals Society of China*, 2016, 26: 3292–3298.
- [21] EL-SAYED M A, HASSANIN H, ESSA K. Bifilm defects and porosity in Al cast alloys [J]. *International Journal of Advance*

- Manufacturing Technology, 2016, 86, 5: 1173–1179.
- [22] RAISZADEH R, GRIFFITHS W D. The behaviour of double oxide film defects in liquid Al alloys under atmospheric and reduced pressures [J]. *Journal of Alloys and Compounds*, 2010, 491: 575–580.
- [23] EL-SAYED M A, GRIFFITHS W D, CAMPBELL J. Hydrogen, bifilms and mechanical properties of Al castings [J]. *International Journal of Cast Metals Research*, 2014, 27(5): 282–287.
- [24] CAMICIA G, TIMELLI G. Grain refinement of gravity die cast secondary AlSi7Cu3Mg alloys for automotive cylinder heads [J]. *Transactions of Nonferrous Metals Society of China*, 2016, 26: 1211–1221.
- [25] WEIBULL W. Statistical distribution function of wide applicability [J]. *Journal of Applied Mechanics*, 1951, 18(3): 293–297
- [26] GREEN N R, CAMPBELL J. Statistical distributions of fracture strengths of cast Al–7Si–Mg alloy [J]. *Materials Science and Engineering A*, 1993, 173: 261–266.
- [27] ASM Specialty handbook, magnesium and magnesium alloys [M]. OH, USA: ASM International, Materials Park, 1999.
- [28] HABASHI F. Alloys: Preparation, properties, applications [M]. Weinheim, Germany: Wiley-VCH, 1998.
- [29] PETERS A T. Degassing magnesium-base alloy: US Patent US3123467 [P]. 1964–03–03.
- [30] WANG L, RHEE H, FELICELLI S D, SABAU A S, BERRY J T. Oxide film and porosity defects in Mg alloy AZ91 [C]//Proc of 3rd International Symposium on Shape Casting. Warrendals: TMS, 2009: 123–130.
- [31] CZERWINSKI F. The reactive element effect on high-temperature oxidation of magnesium [J]. *International Materials Review*, 2015, 60: 264–296.
- [32] TIRYAKIOGLU M, HUDAK D, OKTEN G. On evaluating Weibull fits to mechanical testing data [J]. *Materials Science and Engineering A*, 2009, 527: 397–399.
- [33] CLARK J B. Age hardening in Mg–9wt% Al alloy [J]. *Acta Metallurgica*, 1968, 16(2): 141–152.
- [34] WANG Ya-xiao, ZHOU Ji-xue, WANG Jie, LUO Tian-jiao, YANG Yuan-sheng. Effect of Bi addition on microstructures and mechanical properties of AZ80 magnesium alloy [J]. *Transactions of Nonferrous Metals Society of China*, 2011, 21: 711–716.
- [35] HUANG Hai-jun, CHEN Ti-jun, MA Ying, HAO Yuan. Microstructural evolution during solution treatment of thixoformed AM60B Mg alloy [J]. *Transactions of Nonferrous Metals Society of China*, 2011, 21: 745–753.
- [36] SHEN Z, WAGONER R H, CLARK W A T. Dislocation and grain boundary interaction in metals [J]. *Acta Metallurgica*, 1988, 36(12): 3231–3242.
- [37] CLARCK W A T, WAGONER R H, SHEN Z Y. On the criteria for slip transmission across interfaces in polycrystals [J]. *Scripta Metallurgica et Materialia*, 1992, 26: 203–206.
- [38] YU Kun, RUI Shou-tai, SONG Jue-min, LI Wen-xian, GUO Long. Effect of grain refinement on mechanical properties and microstructure of AZ31 alloy [J]. *Transactions of Nonferrous Metals Society of China*, 2008, 18: 39–43.
- [39] CHEN Y, WANG Q, LIN J, LIU M, HJELLEN J, ROVEN H. Grain refinement of magnesium alloys processed by severe plastic deformation [J]. *Transactions of Nonferrous Metals Society of China*, 2014, 24: 3747–3754.
- [40] WANG Li-ping, CHEN Tian, JIANG Wen-yong, FENG Yi-cheng, CAO Guo-jian, ZHU Yan. Microstructure and mechanical properties of AM60B magnesium alloy prepared by cyclic extrusion compression [J]. *Transactions of Nonferrous Metals Society of China*, 2013, 23: 3200–3205.

T6 热处理对 AM60B 镁合金断裂强度影响的 Weibull 分析

A. H. SHEVIDI, R. TAGHIABADI, A. RAZAGHIAN

Department of Materials Science and Ceramic Engineering,
Imam Khomeini International University, Qazvin, Iran

摘要: 研究 T6 热处理对 AM60B 合金断裂强度和可靠性的影响。在浇铸温度分别为 670、685 和 700 °C，保温时间为 5、10 和 15 min 条件下，制备拉伸试样。用流动性试验测试了合金在不同浇铸温度和保温时间条件下的流动长度。结果表明，最佳的浇铸温度和保温时间分别为 685 °C 和 10 min。拉伸试样的 SEM 断口形貌分析结果显示夹杂的氧化物和与氧化物相关的孔隙是非优化浇铸条件下断裂强度降低的主要因素。将最佳铸造条件下制备的样品采用 T6 热处理制度进行热处理，然后用 Weibull 统计法确定浇铸和热处理条件下断裂强度的分散性。结果表明，T6 热处理制度尽管对平均断裂强度影响较小，但是提高了铸件的可靠性，其 Weibull 模量提高了 75%。显微结构和断口形貌的观察结果显示，热处理后样品的显微组织更加均匀，且消除了粗大的脆性 β 相颗粒，从而提高了铸件的性能。

关键词: Mg–Al 合金；AM60B 合金；压铸；Weibull 分析；断裂强度；流动性

(Edited by Xiang-qun LI)